

# SNARE Protein Recycling by $\alpha$ SNAP and $\beta$ SNAP Supports Synaptic Vesicle Priming

Andrea Burgalossi,<sup>1,7</sup> Sangyong Jung,<sup>1</sup> Guido Meyer,<sup>1,8</sup> Wolf J. Jockusch,<sup>1,9</sup> Olaf Jahn,<sup>2</sup> Holger Taschenberger,<sup>4</sup> Vincent M. O'Connor,<sup>3,10</sup> Tei-ichi Nishiki,<sup>5</sup> Masami Takahashi,<sup>6</sup> Nils Brose,<sup>1,\*</sup> and Jeong-Seop Rhee<sup>1,\*</sup>

<sup>1</sup>Department of Molecular Neurobiology

<sup>2</sup>Proteomics Group and DFG-CMPB

Max Planck Institute of Experimental Medicine, D-37075 Göttingen, Germany

<sup>3</sup>Department of Neurochemistry, Max Planck Institute of Brain Research, D-60528 Frankfurt/Main, Germany

<sup>4</sup>Department of Membrane Biophysics, Max Planck Institute of Biophysical Chemistry, D-37077 Göttingen, Germany

<sup>5</sup>Okayama University Graduate School of Medicine, Dentistry, and Pharmaceutical Sciences, Okayama 700-8558, Japan

<sup>6</sup>Department of Biochemistry, Kitasato University School of Medicine, Kanagawa 228-8555, Japan

<sup>7</sup>Present address: Humboldt University Berlin, Bernstein Center for Computational Neuroscience and Institute for Biology, D-10115 Berlin, Germany

<sup>8</sup>Present address: Harrison Clinical Research, Ely, CB7 4EA, UK

<sup>9</sup>Present address: Carl Zeiss MicroImaging GmbH, D-37081 Göttingen, Germany

<sup>10</sup>Present address: University of Southampton, School of Biological Sciences, Southampton SO16 7PX, UK

\*Correspondence: [rhee@em.mpg.de](mailto:rhee@em.mpg.de) (J.-S.R.), [brose@em.mpg.de](mailto:brose@em.mpg.de) (N.B.)

DOI 10.1016/j.neuron.2010.09.019

## SUMMARY

Neurotransmitter release proceeds by  $\text{Ca}^{2+}$ -triggered, SNARE-complex-dependent synaptic vesicle fusion. After fusion, the ATPase NSF and its cofactors  $\alpha$ - and  $\beta$ SNAP disassemble SNARE complexes, thereby recycling individual SNAREs for subsequent fusion reactions. We examined the effects of genetic perturbation of  $\alpha$ - and  $\beta$ SNAP expression on synaptic vesicle exocytosis, employing a new  $\text{Ca}^{2+}$  uncaging protocol to study synaptic vesicle trafficking, priming, and fusion in small glutamatergic synapses of hippocampal neurons. By characterizing this protocol, we show that synchronous and asynchronous transmitter release involve different  $\text{Ca}^{2+}$  sensors and are not caused by distinct releasable vesicle pools, and that tonic transmitter release is due to ongoing priming and fusion of new synaptic vesicles during high synaptic activity. Our analysis of  $\alpha$ - and  $\beta$ SNAP deletion mutant neurons shows that the two NSF cofactors support synaptic vesicle priming by determining the availability of free SNARE components, particularly during phases of high synaptic activity.

## INTRODUCTION

Neurons signal by releasing neurotransmitters at chemical synapses. The release process is mediated by the fusion of synaptic vesicles (SVs), which is triggered by  $\text{Ca}^{2+}$  ions and executed by SNARE proteins. The latter reside on the SV (Synaptobrevin-2) and synaptic plasma membrane (Syntaxin-1, SNAP-25), and their zipper-like assembly into a tight complex drives the membrane fusion reaction (Jahn and Scheller,

2006). The fidelity of transmitter release in the brain is ensured by regulatory processes that control SV trafficking and SNARE complex function. At active synapses, SVs are continuously supplied to release sites where they undergo a Munc13/CAPS-dependent priming reaction that initiates SNARE complex formation and renders tethered SVs fusion-competent. Only such primed SVs, forming the pool of readily releasable SVs (RRP), can fuse with the plasma membrane upon arrival of an action potential (AP), the concomitant increase of the presynaptic  $\text{Ca}^{2+}$  concentration ( $[\text{Ca}^{2+}]_i$ ), and activation of the putative SV  $\text{Ca}^{2+}$  sensor Synaptotagmin-1 (Syt-1). After fusion, SNARE complex components are dissociated and recycled by an  $\alpha/\beta$ SNAP-NSF complex, and SV membrane and protein components are recovered by endocytosis (Sudhof, 2004; Wojcik and Brose, 2007).

Depending on the activity of a given synapse, different SV trafficking steps become rate limiting for synaptic signaling and kinetically different release mechanisms are employed. This causes short-term changes in synaptic transmission that determine many higher brain functions such as sound localization, sensory adaptation, or even working memory (Wojcik and Brose, 2007). Munc13/CAPS-dependent SV priming, for example, regulates presynaptic depression, facilitation, and augmentation, depending on the synapse type and protein isoform involved (Wojcik and Brose, 2007). At most synapses, two release processes are observed, i.e., synchronous or phasic release that is tightly coupled to incoming APs and asynchronous release that occurs with some delay. The two release processes were suggested to arise from distinct pools of fusion competent SVs (Goda and Stevens, 1994; Sakaba, 2006), although this notion is controversial (Otsu et al., 2004), and the build-up of asynchronous release during AP trains and the concomitant increase of  $[\text{Ca}^{2+}]_i$  is thought to create a tonic release component that contributes to synaptic transmission (Hagler and Goda, 2001; Hefft and Jonas, 2005; Otsu et al., 2004; Sakaba, 2006; Zucker and Lara-Estrella, 1983). Both

phasic and tonic release modes are subject to short-term regulation, and in several cases they are differentially affected by synaptic activity or by genetic perturbation of key SV trafficking steps.

In principle,  $\alpha/\beta$ SNAP-dependent SNARE complex disassembly might influence both phasic and tonic transmitter release modes as well as their short-term plasticity. Indeed, functional inactivation of the  $\alpha/\beta$ SNAP-dependent SNARE complex disassembly ATPase NSF in temperature-sensitive *Drosophila* mutants leads to a progressive defect in transmitter release and consequent paralysis (Littleton et al., 2001). Constitutive deletion of  $\alpha$ SNAP in mice leads to embryonic lethality, and a 50% reduction of  $\alpha$ SNAP expression in the hypomorphic "Hydrocephaly with Hop-gait" (HYH) mutant (Chae et al., 2004; Hong et al., 2004) causes complex and as yet poorly understood changes in apical protein localization and cell fate determination in neuroepithelial cells. A detailed genetic analysis of the function of  $\alpha$ - and  $\beta$ SNAP in transmitter release from mammalian neurons has not been performed to date.

Because of their interdependence, it has been very difficult to study individual SV trafficking steps, their molecular basis, their contribution to synchronous, asynchronous, and tonic release, and their role in presynaptic short-term plasticity, particularly in small glutamatergic synapses, which are the most abundant in the mammalian brain. We have circumvented this problem by stimulating transmitter release in autaptic mouse hippocampal glutamatergic neurons using UV-flash mediated  $\text{Ca}^{2+}$  uncaging (Sakaba, 2008; Schleggenburger and Neher, 2000). This bypasses  $\text{Ca}^{2+}$  channel activation and coupling to the release machinery, and allowed us to study individual steps of the SV cycle in hippocampal synapses at an unprecedented level of detail. We applied the  $\text{Ca}^{2+}$  uncaging method to determine SV dynamics in neurons of previously described mouse deletion mutants (CAPS-1/2, Munc13-1/2, Syt-1) and to study the functional role of  $\alpha$ - and  $\beta$ SNAP in presynaptic function and short-term plasticity using novel mutant mice. Our study provides important new insights into the nature of synchronous, asynchronous, and tonic transmitter release, and the role of SNARE protein recycling in determining the fidelity of synaptic transmission during high synaptic activity.

## RESULTS

### $\text{Ca}^{2+}$ Uncaging in Autaptic Glutamatergic Hippocampal Neurons

We chose cultured autaptic hippocampal neurons as our model system to establish a  $\text{Ca}^{2+}$  uncaging protocol for the study of small glutamatergic synapses. Synaptic transmission in this preparation has mainly been studied by inducing APs through a patch pipette while the RRP has been determined with hyper-tonic sucrose solution (HSS) (Jockusch et al., 2007). To test whether  $\text{Ca}^{2+}$  uncaging can be used to release the entire RRP, wild-type (WT) neurons were loaded with NP-EGTA, Mag-Fura-2, and Fura-4F (Figure 1B).  $[\text{Ca}^{2+}]_i$  was measured in the distal dendrite (third order branches) as routine measurements of  $[\text{Ca}^{2+}]_i$  in axons or presynaptic terminals was not feasible. After 20 min of cell dialysis, a brief UV flash was delivered, which

elevated  $[\text{Ca}^{2+}]_i$  to  $\sim 30 \mu\text{M}$ . Longer dialysis times were only necessary in neurons that had been cultured for more than 10 days due to the higher axonal complexity. We therefore focused our study on neurons at days in vitro 7–10.

Rapid elevation of  $[\text{Ca}^{2+}]_i$  to 20–30  $\mu\text{M}$  triggered a fast postsynaptic current (EPSC) within  $\sim 1$  ms (Figures 1A–1C), followed by a long-lasting EPSC. The amplitude of the fast flash-evoked EPSC was three times larger than the AP-evoked EPSC amplitude. The EPSC induced by  $\text{Ca}^{2+}$  uncaging was abolished by AMPA receptor blockers and in Munc13-1/2 double KO (Munc13-DKO) neurons, which are deficient in transmitter release (Wojcik and Brose, 2007) (see Figure S1A available online). APs (Figure 1A) and HSS (Figure S1C) applied after the flash failed to trigger additional glutamate release.

The lack of AP evoked release after  $\text{Ca}^{2+}$  uncaging was not due to a failure of AP propagation since AP-triggered EPSCs could be reliably evoked in earlier phases of cell perfusion, during which the caged  $\text{Ca}^{2+}$  had entered the axon but not all presynaptic terminals (Figure S1B). Likewise, the lack of AP-evoked release after  $\text{Ca}^{2+}$  uncaging is unlikely to be caused solely by  $\text{Ca}^{2+}$ -dependent inactivation of presynaptic  $\text{Ca}^{2+}$  channels due to elevated postflash  $[\text{Ca}^{2+}]_i$ . We addressed this issue indirectly by examining changes in somatic voltage dependent  $\text{Ca}^{2+}$  currents of the N-, P/Q-, and R-types before and after  $\text{Ca}^{2+}$  uncaging in the presence of 5  $\mu\text{M}$  nimodipine, an L-type  $\text{Ca}^{2+}$  channel blocker. For a postflash  $[\text{Ca}^{2+}]_i$  of  $\sim 20 \mu\text{M}$ , we measured a reduction of somatic  $\text{Ca}^{2+}$  currents by  $\sim 50\%$  (data not shown). On the other hand, AP-evoked EPSCs after flash were reduced by more than 99% (i.e., to the noise level) as compared to preflash control values (Figure 1A). Elevated  $[\text{Ca}^{2+}]_i$  after  $\text{Ca}^{2+}$  uncaging reduces the number of  $\text{Ca}^{2+}$  channels available for opening during a presynaptic AP. The effect of a reduced number of open  $\text{Ca}^{2+}$  channels on transmitter release depends on the coupling between  $\text{Ca}^{2+}$  channels and the vesicle fusion machinery. If many  $\text{Ca}^{2+}$  channels control the fusion of a single SV, the cooperativity between  $\text{Ca}^{2+}$  current and transmitter release will be close to the biochemical cooperativity, i.e.,  $\sim 3$ , but if only very few  $\text{Ca}^{2+}$  channels control the fusion of a single SV, the cooperativity between  $\text{Ca}^{2+}$  current and transmitter release will approach 1. Thus, a relative reduction in  $\text{Ca}^{2+}$  currents by a factor of 0.5 ( $\sim 50\%$ ), as we observed, is expected to reduce the EPSC by a factor of  $0.5^1$ – $0.5^3$  or 0.5–0.125. To explain the reduction of the postflash EPSC by a factor of 0.01 (99%) seen in our experiments (Figure 1A), one would need to assume a reduction of  $\text{Ca}^{2+}$  currents by a factor of 0.01–0.22, which was not the case. On aggregate, above findings show that under our assay conditions NP-EGTA had effectively diffused into all presynaptic terminals and that elevation of  $[\text{Ca}^{2+}]_i$  by  $\text{Ca}^{2+}$  uncaging induced the release of the entire RRP. Thus, EPSCs induced by  $\text{Ca}^{2+}$  uncaging are a novel readout of the  $\text{Ca}^{2+}$  dependent release of the entire RRP in hippocampal neurons.

As RRP release by  $\text{Ca}^{2+}$  uncaging occludes HSS-induced RRP release (Figure S1C), we next tested the reverse by first triggering RRP release with HSS and then delivering an AP followed by a flash in the continuous presence of HSS. Although a single AP did not induce any release after RRP depletion by HSS,  $\text{Ca}^{2+}$  uncaging still evoked a prominent but slow EPSC,

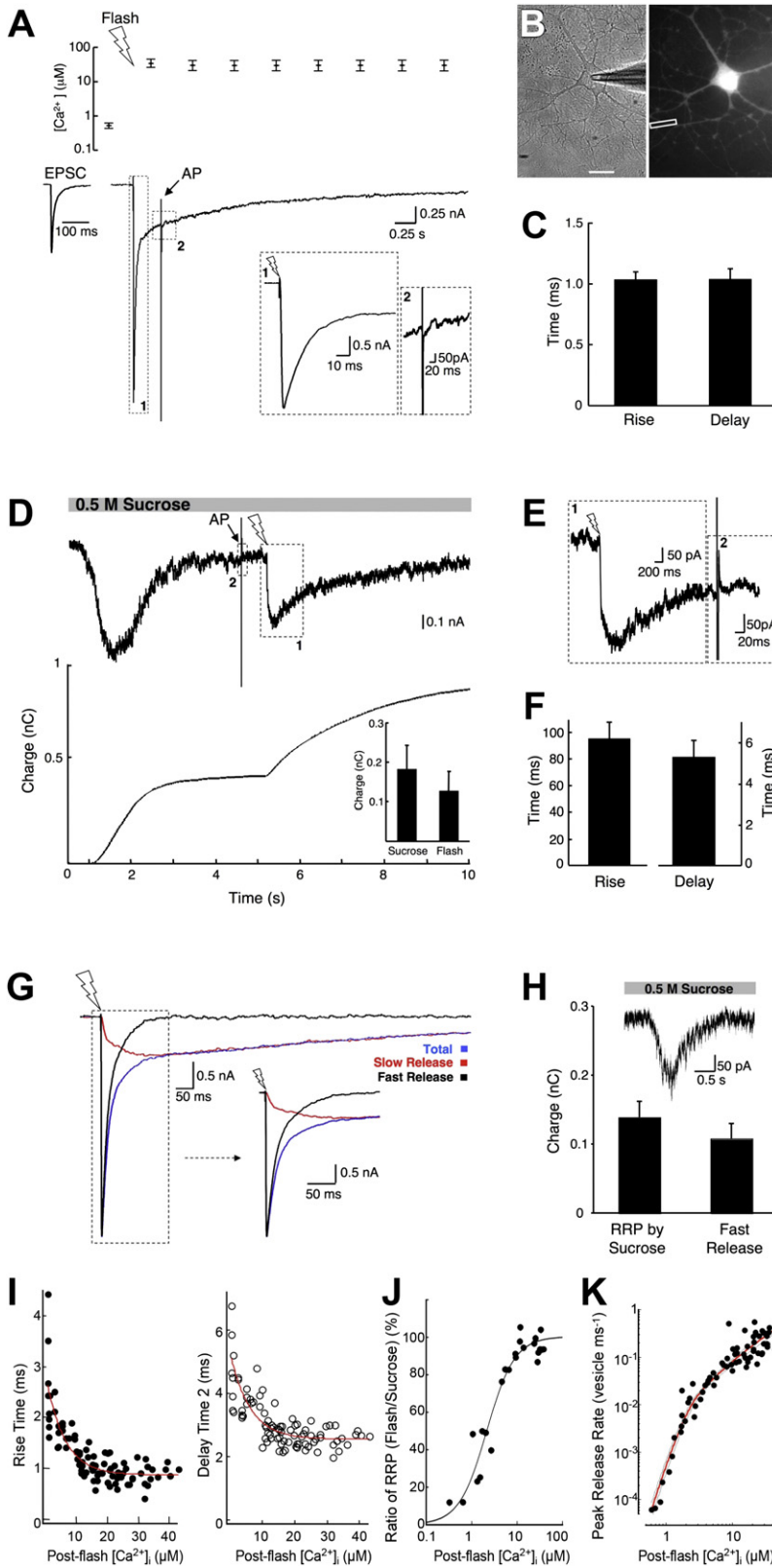


**Figure 1. Ca<sup>2+</sup> Uncaging in Hippocampal WT Neurons**

(A) Change in [Ca<sup>2+</sup>]<sub>i</sub> and release evoked by Ca<sup>2+</sup> uncaging. The upper panel shows [Ca<sup>2+</sup>]<sub>i</sub> before and after the flash (flash icon). The lower traces show averaged EPSC and flash-induced responses (n = 13). Insets are magnifications of marked sections 1 and 2.

(B) Transmission and fluorescence images of a dialyzed cell. Scale bar represents 20 μm.

(C) Average rise and delay times of flash responses shown in (A) (n = 13).

(D) Representative HSS response and flash-evoked response in the presence of HSS (top) and corresponding total synaptic charge transfer (bottom). The inset shows the quantification of total charges induced by HSS and flash (n = 8).

(E) Magnification of the marked sections 1 and 2 in (D).

(F) Average rise and delay times of flash responses shown in (D).

(G) Superimposed average traces for total flash response (blue), flash response in the presence of HSS (red), and fast flash response (black; difference between blue and red traces) (n = 7). AP artifacts (200 ms after flash) were removed. The inset shows a magnification of the marked section.

(H) Quantification of total synaptic charges during fast release and HSS-induced release in the same subset of neurons (n = 7). A representative trace of HSS-induced release is shown above the bar graph.

(I) [Ca<sup>2+</sup>]<sub>i</sub> dependence of rise times (10%–90%, left panel) and delay time 2 (right panel) of transmitter release triggered by flash in WT neurons (68 flash-evoked EPSCs recorded in 34 neurons). The delay time 2 was calculated from the onset of release to the peak of the response.

(J) [Ca<sup>2+</sup>]<sub>i</sub> dependence of transmitter release. Each dot represents the measurement from one independent cell. For each cell, the flash induced current triggered at the indicated [Ca<sup>2+</sup>]<sub>i</sub> was divided by the HSS-induced current measured before the flash for normalization purposes.

(K) Release rate per vesicle plotted as a function of post-flash [Ca<sup>2+</sup>]<sub>i</sub> (pooled data representing 68 flash-evoked EPSCs recorded in 34 neurons). Solid and dotted lines represent kinetic model fits and 95% confidence limits, respectively. A five-site kinetic model (Schneppenburger and Neher, 2000) was used to fit the data, with the fusion rate  $\gamma$  and the cooperativity factor  $b$  fixed to 6 ms<sup>-1</sup> and 0.25, respectively.

Error bars indicate standard error of the mean. The arrow and flash-icon indicate AP induction and flash, respectively. See also Figure S1.

whose total charge was 63% of the HSS-triggered EPSC (Figures 1D and 1E). When compared to the flash-induced release in the absence of HSS (Figure 1A), the flash-induced release in the presence of HSS completely lacked the fast component. It showed much slower delay times (i.e., onset of release after flash) and rise times (delay time,  $5.2 \pm 0.7$  ms; rise time,  $95 \pm 11$  ms; Figure 1F) but had an identical decay time course (Figure 1G). Similarly, a high-frequency AP train applied after RRP depletion by HSS induced only slow release without a fast component (Figure S1D). The slower kinetics of release observed in the presence of HSS after RRP depletion are not due to adverse effects of the osmotic shock on the release machinery since  $\text{Ca}^{2+}$  uncaging in the presence of HSS, but before RRP depletion, induced SV fusion with very fast kinetics (Figure S1E).

The experiments noted above show that after HSS-induced RRP depletion the elevation of  $[\text{Ca}^{2+}]_i$  by  $\text{Ca}^{2+}$  uncaging or by high-frequency stimuli can only induce additional “slow” release. The release triggered by  $\text{Ca}^{2+}$  uncaging thus consists of two release processes, a “fast” release that is selectively abolished by HSS application, and a slow release that is HSS insensitive. We subtracted the flash response obtained in the presence of HSS from the one obtained under normal conditions to estimate the HSS-sensitive component (Figure 1G). The kinetics of the slow component were calculated from independent experiments on WT neurons as run-down of synaptic responses usually prevented a systematic estimate of the kinetics of slow release from the same cells in which flash-evoked release was also assessed. These independent experiments were performed on cells with similar EPSC amplitudes, RRP sizes, and postuncaging  $\text{Ca}^{2+}$  levels as the ones in which flash-evoked responses were measured. In a set of cells, in which synaptic transmission after the first flash recovered to preflash levels, we were able to assess the slow release component from the same cell by applying a first flash followed by a second flash in the presence of HSS. The kinetics of the slow components obtained from independent experiments on different WT cells (Figure 1G) and from the same cells (delay time,  $6.4 \pm 0.74$  ms,  $n = 7$ ; rise time,  $103.7 \pm 19.52$  ms,  $n = 7$ ) did not differ and yielded similar results when a subtraction from total flash-evoked release was performed. The total charge of the isolated fast, HSS-sensitive component of the flash response matched the RRP size measured by HSS application in the same subset of neurons (HSS,  $0.13 \pm 0.23$  nC; fast flash response,  $0.10 \pm 0.22$  nC) (Figure 1H), indicating that the fast phase of the flash response reports total RRP release.

To study the  $\text{Ca}^{2+}$  dependence of synaptic release and depletion of the RRP, we recorded EPSCs induced at varying flash intensities (Figures 1I–1K). We observed a striking  $[\text{Ca}^{2+}]_i$  dependence of the EPSCs and found that  $[\text{Ca}^{2+}]_i$  levels of  $\sim 15$ – $20$   $\mu\text{M}$  were sufficient to trigger maximal responses with regard to amplitude and kinetics of synchronous release (Figure 1I) and to RRP depletion (Figure 1J). We estimated peak release rates as a function of  $[\text{Ca}^{2+}]_i$  by deconvolution of flash evoked EPSCs using a measured miniature EPSC (mEPSC) waveform, and divided the corresponding values by the RRP size of the given cell to yield the peak release rate per SV (Figure 1K). A double-logarithmic plot of the latter values as a function of  $[\text{Ca}^{2+}]_i$  had

a slope of  $\sim 3$  (Figure 1K), which is only slightly lower than corresponding data obtained in the calyx of Held (Young and Neher, 2009). In addition, the threshold  $[\text{Ca}^{2+}]_i$  value at which release can be triggered in hippocampal autaptic neurons is slightly lower than corresponding values obtained in the calyx of Held (Schneeggenburger and Neher, 2000; Neher and Sakaba, 2008). These differences likely arise from a slight underestimation of the actual  $[\text{Ca}^{2+}]_i$  at presynaptic terminals by measuring  $[\text{Ca}^{2+}]_i$  in distal dendrites because dendrites are compartmentalized and contain multiple  $\text{Ca}^{2+}$  buffers, but we cannot exclude that intrinsic differences exist between autaptic hippocampal neurons and the calyx of Held with regard to the  $[\text{Ca}^{2+}]_i$  dependence of transmitter release. In any case, our data show that  $[\text{Ca}^{2+}]_i$  levels of  $>20$   $\mu\text{M}$ , which we routinely triggered by  $\text{Ca}^{2+}$  uncaging, are sufficient to evoke maximal transmitter release in autaptic hippocampal neurons.

Above findings show that rapid elevation of  $[\text{Ca}^{2+}]_i$  to  $>20$   $\mu\text{M}$  by  $\text{Ca}^{2+}$  uncaging induces the rapid discharge of the RRP within 200 ms and a much slower release process that decays with a slower time constant ( $\tau = 1.34$  s,  $n = 13$ ). While this slower component might represent release from a “reluctantly” releasing SV pool, the fact that neither APs nor HSS triggered additional release after a  $\text{Ca}^{2+}$  uncaging stimulus (Figure 1A and Figure S1C) indicates that  $\text{Ca}^{2+}$  uncaging is sufficient to deplete all primed SVs in the autaptic preparation (see also Wadel et al., 2007). Hence, the slow release phase observed by  $\text{Ca}^{2+}$  uncaging during HSS stimulation is most likely due to ongoing priming and fusion of incoming SVs and not to an already primed SV pool. Its time course can be explained by the initial release of the very small RRP that remains in the presence of HSS, followed by a strong  $\text{Ca}^{2+}$  dependent increase in SV priming, which determines the rising phase of the slow response, and the subsequent depletion of reserve SVs in the continued presence of high  $[\text{Ca}^{2+}]_i$ , which determines the decay kinetics of the slow response (Neher and Sakaba, 2008). Thus, the  $\text{Ca}^{2+}$  uncaging protocol allows to distinguish between the RRP itself, its replenishment by newly primed SVs, and the exhaustion of reserve SV pools.

We next validated the  $\text{Ca}^{2+}$  uncaging protocol by examining two well characterized KO models, CAPS1/2 double KOs (CAPS-DKO) (Jockusch et al., 2007) and Syt-1-KOs (Geppert et al., 1994). CAPS-DKO neurons are deficient in SV priming. Some 40% of CAPS-DKO neurons are “silent,” do not release any transmitter in response to single APs or HSS, and show only tonic release during high-frequency AP trains (Figure 2D). This tonic release is also seen in WT cells, where it is superimposed with phasic AP-coupled release and attributed to a primed SV pool with a different  $\text{Ca}^{2+}$  sensitivity (Figure 2B) (Zucker and Lara-Estrella, 1983). To study the nature of tonic release, we applied the  $\text{Ca}^{2+}$  uncaging protocol to silent CAPS-DKO neurons.  $\text{Ca}^{2+}$  uncaging in CAPS-DKO cells induced only slow release (Figures 2A, 2C, 2E, and 2F). This slow release had similar kinetics as the slow release phase in WT neurons, and cumulative release had a similar single exponential time course (WT,  $\tau = 1.34$  s; CAPS-DKO,  $\tau = 1.32$  s; Figures S1F and S1G), indicating that the slow release observed in CAPS-DKO neurons upon  $\text{Ca}^{2+}$  uncaging and tonic release triggered by high-frequency AP trains originate from the

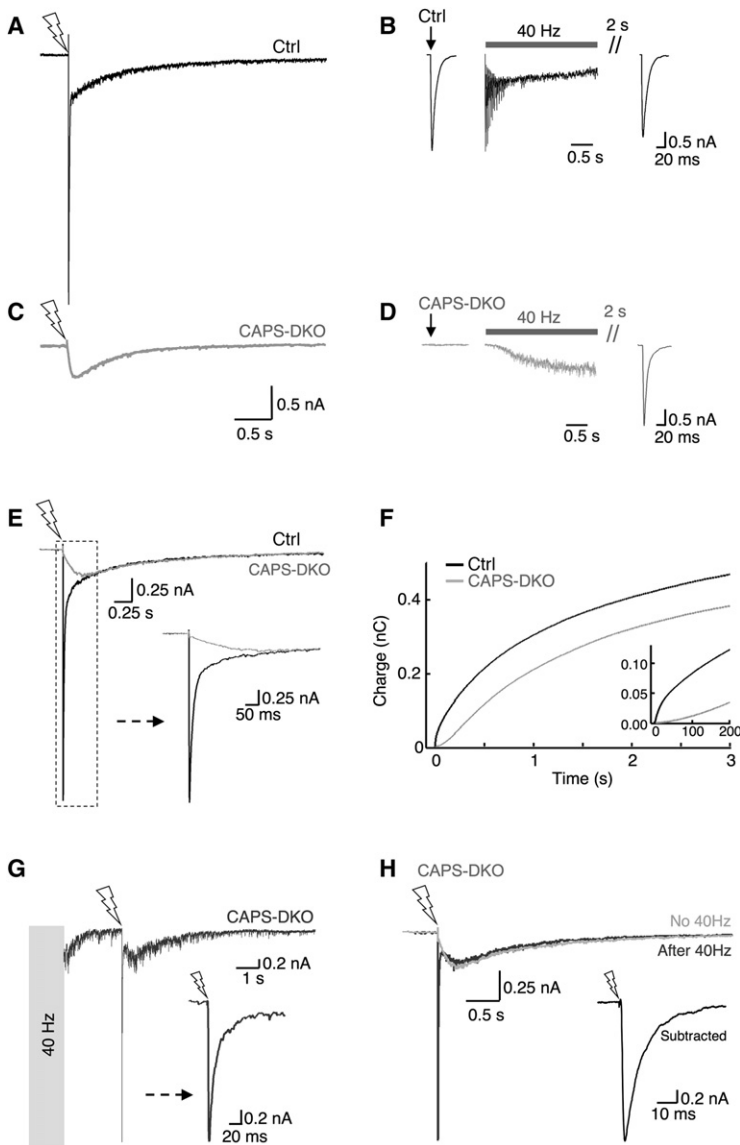


### Figure 2. $\text{Ca}^{2+}$ Uncaging in CAPS-DKO Neurons

(A and C) Representative flash responses of Ctrl (A) and silent CAPS-DKO neurons (C). AP artifacts (200 ms after flash) were removed.

(B and D) Representative current traces from control (B) and silent CAPS-DKO neurons (D) recorded before, during, and 2 s after a 40 Hz AP train of 2.5 s.

(E) Superimposed average traces for flash response in Ctrl ( $n = 14$ ) and CAPS-DKO neurons ( $n = 11$ ). The inset shows a magnification of the marked section.

(F) Total synaptic charge transfer for data shown in (E). The inset shows a magnification of the early phase of the curve.

(G) Representative recording from a CAPS-DKO neuron where the flash was delivered 2 s after a 40 Hz stimulation for 2.5 s (gray box). The inset shows a magnification of the fast release phase induced by the flash.

(H) Superimposed average traces for flash response in CAPS-DKO neurons with (dark gray,  $n = 5$ ) or without (light gray, cells from (C)) a preceding 40 Hz stimulation. The inset shows a magnification of the fast release phase induced by the flash (obtained by subtraction of the two traces).

The flash-icon indicates the flash. See also Figure S1.

WT cells (CAPS-DKO; delay time,  $1.10 \pm 0.07$  ms; rise time,  $1.02 \pm 0.07$  ms;  $n = 5$ ), followed by slow release (Figure 2G). Size and kinetics of slow release from CAPS-DKO cells after a 40 Hz AP train were identical to those of resting CAPS-DKO cells (Figure 2H), supporting the notion that tonic release during high-frequency stimulation and slow release triggered by  $\text{Ca}^{2+}$  uncaging are due to the ongoing fusion of newly primed SVs.

In the absence of the putative  $\text{Ca}^{2+}$  sensor Syt-1, hippocampal neurons display only asynchronous release in response to a single AP (Figure 3B). To examine the  $\text{Ca}^{2+}$ -sensor function of Syt-1 and to elucidate the nature of asynchronous release and its relationship with tonic release, we studied Syt-1-KO neurons using the  $\text{Ca}^{2+}$  uncaging protocol.  $\text{Ca}^{2+}$  uncaging elicited fast and slow release components in both Syt-1-KO and Ctrl neurons (Figures 3A and 3B). However, fast release was delayed in Syt-1-KO

neurons (delay times; Ctrl,  $0.98 \pm 0.05$  ms; Syt-1-KO,  $2.63 \pm 0.25$  ms), and EPSC rise times were slower (Ctrl,  $0.91 \pm 0.14$  ms; Syt-1-KO,  $3.99 \pm 0.38$  ms) (Figures 3E–3G). To probe the  $\text{Ca}^{2+}$  dependence of release at Syt-1-KO synapses, we performed a titration of flash-evoked release as a function of  $[\text{Ca}^{2+}]_i$  by varying the levels of uncaged  $[\text{Ca}^{2+}]_i$  (Figures 3H and 3I). Syt-1-KO neurons showed a clear  $[\text{Ca}^{2+}]_i$  sensitivity of release, as indicated by the  $[\text{Ca}^{2+}]_i$  dependence of release kinetics and peak release rate per SV. However, compared to WT neurons (Figures 1I–1K), the  $\text{Ca}^{2+}$  sensitivity of release in Syt-1-KO neurons was drastically altered, as rise times and delay times were increased and the double-logarithmic plot of the peak release rate per SV as a function of  $[\text{Ca}^{2+}]_i$  had a reduced slope with higher release rates at low  $[\text{Ca}^{2+}]_i$  levels and lower release rates at higher  $[\text{Ca}^{2+}]_i$  levels (Figure 3H and 3I). These findings show that Syt-1 acts as a  $\text{Ca}^{2+}$  sensor of release in whose

continuous release of newly primed SVs and not from an already primed SV pool. Interestingly, the slow flash induced discharge of SVs in CAPS-DKO neurons was delayed by  $\sim 180$  ms as compared to Ctrl neurons (time to peak; Ctrl, 122 ms; CAPS-DKO 305 ms; Figures S1F and S1G), which is consistent with earlier data on calcimycin triggered release from CAPS-DKO cells (Jockusch et al., 2007). Thus, 180 ms correspond to the average time required to build up newly primed SVs in CAPS-DKO synapses upon  $\text{Ca}^{2+}$  uncaging, which likely involves the  $\text{Ca}^{2+}$ -dependent action of Munc13s (Jockusch et al., 2007). Shortly after a 40 Hz AP train silent CAPS-DKO neurons displayed phasic EPSCs, indicating that brief increases in  $[\text{Ca}^{2+}]_i$  can transiently restore and stabilize the RRP in these neurons (Figure 2D) (Jockusch et al., 2007). Consistent with this,  $\text{Ca}^{2+}$  uncaging after a 40 Hz AP train triggered a fast release phase in CAPS-DKO neurons, which showed similar kinetics as seen in

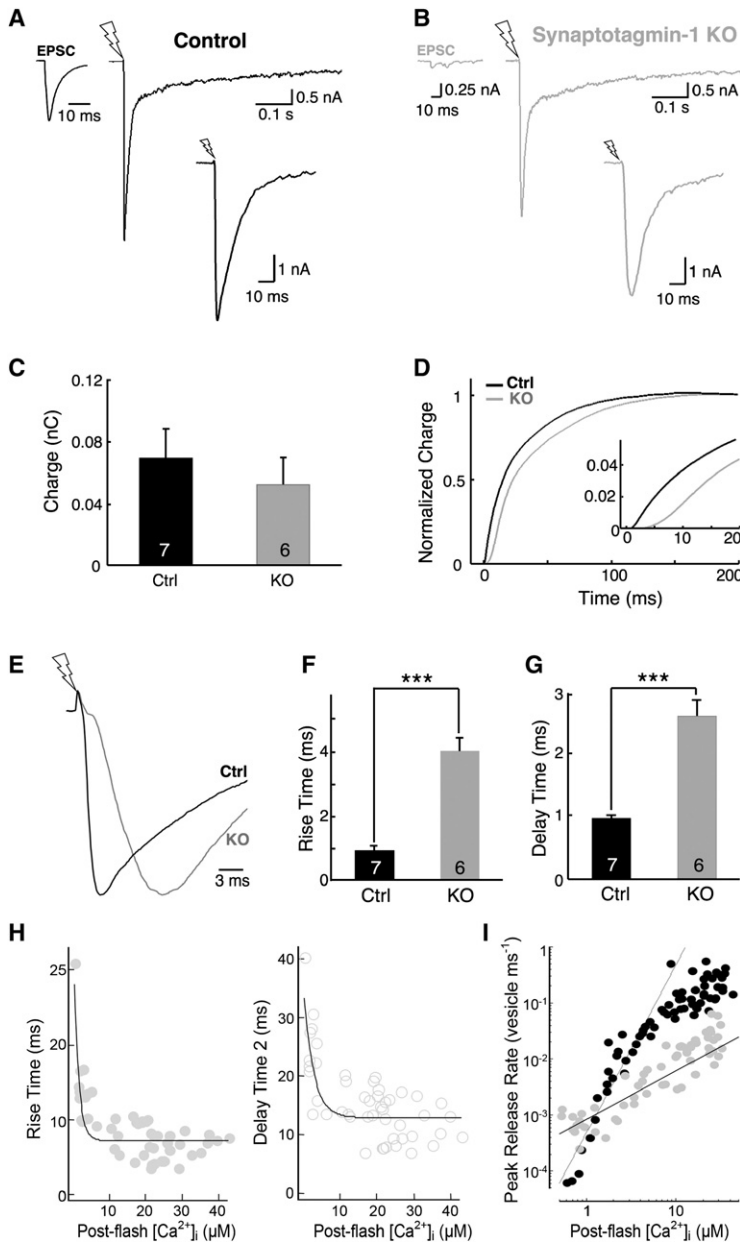


**Figure 3.  $Ca^{2+}$  Uncaging in Syt-1-KO Neurons**

(A and B) Representative traces of flash responses in Ctrl (A) and Syt-1-KO neurons (B). AP artifacts 200 ms after the flash were removed. The insets show traces obtained by subtracting responses in the presence of HSS (Figure S2C) from the total flash responses.

(C) Total charge transfer during the fast flash response in Ctrl ( $n = 7$ ) and Syt-1-KO neurons ( $n = 6$ ).

(D) Normalized synaptic charge transfer of data shown in (C). The inset shows a magnification of the early phase of the curve.

(E) Amplitude-normalized traces of flash responses in Ctrl and Syt-1-KO neurons (C).

(F, G) Average rise (F) and delay times (G) of flash responses shown in (E).

(H)  $[Ca^{2+}]_i$  dependence of rise times (10%–90%, left panel) and delay time 2 (right panel) of transmitter release triggered by flash in Syt-1-KO neurons (59 flash-evoked EPSCs recorded in 43 neurons). The delay time 2 was calculated from the onset of release to the peak of the response.

(I) Release rate per vesicle plotted as a function of postflash  $[Ca^{2+}]_i$  for Ctrl (black filled circles, same data as shown in Figure 1K) and Syt-1-KO neurons (filled gray circles). Line fits of release rates versus  $[Ca^{2+}]_i$  in double-logarithmic plots (dotted and solid lines) yielded slope values of  $\sim 3.0$  and  $\sim 0.9$  for  $[Ca^{2+}]_i$  elevations between  $\sim 0.6$  and  $\sim 6 \mu M$  in Ctrl and Syt-1-KO neurons, respectively.

Error bars indicate standard error of the mean. The flash-icon indicates flash. See also Figure S1.

were not statistically different from Ctrl values (Ctrl,  $\tau_f = 7.8 \pm 1.24$  ms, 33%,  $\tau_s = 43.0 \pm 7.1$  ms, 67%; Syt-1-KO,  $\tau_f = 8.6 \pm 1.1$  ms, 43%,  $\tau_s = 42.9 \pm 5.2$  ms, 57%). Thus, Syt-1-KO neurons exhibit the typical heterogeneity of primed SV pools, much like control cells. Previous studies indicated the existence of Syt-1-sensitive and Syt-1-insensitive primed SV pools, the latter of which was suggested to cause asynchronous and tonic transmitter release (Maximov and Sudhof, 2005). Our data show that even the slow release component measured by  $Ca^{2+}$  uncaging in the presence of HSS is delayed in Syt-1-KO cells (Ctrl,  $4.2 \pm 0.5$  ms; Syt-1-KO,  $9.9 \pm 2.2$  ms; Figure S1H). In view of this finding, which indicates that tonically released SVs are also sensitive to Syt-1 loss, and the fact that Syt-1-KO neurons have an RRP that is released quickly by  $Ca^{2+}$  uncaging, the asynchronous release triggered by single APs in Syt-

1-KO neurons is most likely due to a change in  $Ca^{2+}$  sensing by a sensor other than Syt-1, rather than to a unique primed SV pool.

absence a more  $[Ca^{2+}]_i$  sensitive but less effective and as yet unidentified  $Ca^{2+}$  sensor is operational.

The RRP size estimated by  $Ca^{2+}$  uncaging was not significantly reduced in Syt-1-KO cells (Ctrl,  $0.069 \pm 0.017$  nC; Syt-1-KO,  $0.052 \pm 0.018$  nC) (Figure 3C). While EPSC amplitudes were drastically reduced in Syt-1-KO neurons (Ctrl,  $2.0 \pm 0.17$  nA,  $n = 39$ ; Syt-1-KO,  $0.19 \pm 0.03$  nA,  $n = 36$ ), EPSC charges measured within 1 s after the APs were only reduced to  $\sim 30\%$  of control levels (Ctrl,  $0.017 \pm 0.0015$  nC,  $n = 39$ ; Syt-1-KO,  $0.0054 \pm 0.00049$  nC,  $n = 36$ ). Interestingly, the cumulative charge triggered by RRP release from Syt-1-KO cells upon  $Ca^{2+}$  uncaging still followed a double exponential time course (Figure 3D), and the time constants and relative contributions of the two phases

### Endogenous $\alpha$ - and $\beta$ -SNAP in Mouse Brain and Cultured Hippocampal Neurons

$\alpha$ - and  $\beta$ SNAP are highly homologous to each other but distinct from the third SNAP family member,  $\gamma$ SNAP (Clary et al., 1990; Nishiki et al., 2001; Peter et al., 1998). To characterize  $\alpha$ - and  $\beta$ SNAP, we first studied their distribution in subcellular fractions of mouse brain (Figure S2A).  $\alpha$ - and  $\beta$ SNAP were detected in substantial amounts in all subcellular membrane and soluble fractions, showed a very similar distribution pattern, and were only moderately enriched in synaptic fractions (Figure S2A).

We next studied the developmental expression profiles of  $\alpha$ - and  $\beta$ SNAP in mouse brain by western blotting (Figure S3B). While  $\alpha$ SNAP levels were rather constant throughout embryonic and postnatal development and increased only moderately in later stages,  $\beta$ SNAP expression first appeared around birth and increased during the first 2–3 weeks of postnatal life, which is reminiscent of synaptic marker proteins. Likewise, we found that in primary cultured neurons  $\beta$ SNAP expression is strongly upregulated during the first 2–3 weeks of in vitro development, while  $\alpha$ SNAP expression shows only moderate changes (Figure S3C).

### SNARE Protein Binding by $\alpha$ - and $\beta$ SNAP

We next examined whether  $\alpha$ - and  $\beta$ SNAP differ with regard to SNARE complex binding by comparing their ability to be incorporated into the complex containing SNAPs, NSF, and the SNARE complex (the 20S complex), and to mediate ATP-dependent disassembly of SNARE complexes (Sollner et al., 1993). Recombinant Myc-tagged NSF, His-tagged  $\alpha$ - or  $\beta$ SNAP, and brain membrane extract were incubated together in the presence of ATP/EDTA, which stabilizes 20S complexes. Stably assembled 20S complexes were then immunopurified via the Myc-tag of NSF and specifically eluted with ATP/Mg<sup>2+</sup>, and the ATP-eluted fractions were separated by SDS-PAGE (Figure S2D). Coomassie stained bands that were absent from control samples were excised and analyzed by mass spectrometry. When  $\alpha$ - or  $\beta$ SNAP were included in the assay, we identified the neuronal SNAREs Synaptobrevin-2 and SNAP-25 in both eluted fractions at the expected molecular weights. We were not able to identify Syntaxin-1 by mass spectrometry because the excess of SNAPs used in the assay masked the co-migrating Syntaxin-1. However, Syntaxin-1 was readily identified by western blotting (Figure S2E). In contrast, Synaptotagmin-1 was not detectable in eluted fractions (Figure S2E), even after long blot exposure (data not shown). This is consistent with the notion that Synaptotagmin-1 and SNAPs compete for the same binding site on the SNARE complex (McMahon et al., 1995). As  $\alpha$ - and  $\beta$ SNAP are coexpressed in brain, we performed a parallel assay with both isoforms included in a 1:1 ratio. We found that both isoforms together were also very efficient in pulling-down SNARE proteins from brain membrane extracts (Figure S2E).

### $\alpha$ - and $\beta$ SNAP Function

While most previously published studies indicated that increased  $\alpha$ SNAP levels promote vesicle fusion (Babcock et al., 2004; DeBello et al., 1995; He et al., 1999; Morgan and Burgoyne, 1995; Xu et al., 2002), some reported that high  $\alpha$ SNAP levels can also inhibit fusion (e.g., Barszczewski et al., 2008). So far, the effect of  $\alpha$ - and  $\beta$ SNAP overexpression in central mammalian synapses has not been investigated. We therefore employed the Semliki Forest Virus overexpression system to analyze excitatory synaptic transmission in  $\alpha$ - or  $\beta$ SNAP overexpressing autaptic hippocampal neurons. Using this method,  $\alpha$ - or  $\beta$ SNAP were overexpressed far above WT levels (>3-fold) (data not shown). Electrophysiological analyses showed that such strong overexpression of  $\alpha$ - or  $\beta$ SNAP in WT neurons had no effect on glutamatergic synaptic transmission (Figure S3).

The levels of free SNARE proteins at synapses and their recovery from “spent” complexes that participated in fusion reactions and remain in the plasma membrane are predicted to limit the size of the RRP and the rate of its recovery after depletion (DeBello et al., 1995; Xu et al., 2002). To examine the role of SNARE recycling and free SNARE protein levels in SV trafficking, we studied mutant mice with reduced  $\alpha$ - and  $\beta$ SNAP expression levels. For this purpose, we generated a novel  $\beta$ SNAP-KO mouse line (Figure S4), crossed it with a hypomorphic  $\alpha$ SNAP mouse mutant (HYH) (Chae et al., 2004; Hong et al., 2004), and analyzed neurons of the corresponding single and double mutant (DMut) mice.

The hypomorph HYH mutant was used because the  $\alpha$ SNAP-KO is embryonically lethal, which is most likely due to the facts that  $\alpha$ SNAP is essential for multiple cellular membrane trafficking steps and ubiquitously expressed already during early development (Chae et al., 2004; Hong et al., 2004; Whiteheart et al., 1993). HYH is a recessive missense mutation (M105I) in the  $\alpha$ SNAP protein that arose spontaneously in C75L/10J mice. It results in a 50% reduction of  $\alpha$ SNAP levels as a consequence of either mRNA or protein instability without affecting protein function (Chae et al., 2004). Despite the reduction in total  $\alpha$ SNAP levels, basic synaptic transmission and synaptic plasticity was normal in HYH neurons (Figures S5A–S5E). Accordingly, we found that the HYH mutation did not disrupt the in vitro interaction of  $\alpha$ SNAP with previously identified putative interaction partners (Martin et al., 2006) (data not shown). In order to exclude possible dominant-negative effects of the HYH mutation on synaptic function, we overexpressed the HYH  $\alpha$ SNAP variant in autaptic hippocampal WT neurons and analyzed glutamatergic synaptic transmission. Basic parameters of synaptic transmission and synaptic plasticity were not altered in HYH overexpressing neurons (Figures S5F–S5J).

In contrast to  $\alpha$ SNAP,  $\beta$ SNAP expression is restricted to the brain and only detectable postnatally (Figure S2B) (Nishiki et al., 2001; Whiteheart et al., 1993). Accordingly,  $\beta$ SNAP-KOs showed no overt phenotypic changes at birth. However, from postnatal day 11 onward, they developed severe recurrent epileptic seizures, which lasted for up to 1 min and were followed by a long period of ataxia. Occasionally,  $\beta$ SNAP-KO mice did not recover and died. The onset of the epileptic phenotype in  $\beta$ SNAP-KOs is consistent with the developmental expression pattern of  $\beta$ SNAP (Figure S2B). The  $\beta$ SNAP deficient brains did not show any morphological alterations (data not shown), and no changes in the expression levels of a large number of functionally related proteins were observed (Figures S6A and S6B), indicating that at the morphological and biochemical levels  $\beta$ SNAP-KO brains are very similar to WT brains. To study the effect of the  $\beta$ SNAP deletion on synaptic function, we analyzed glutamatergic synaptic transmission in autaptic hippocampal neurons. The  $\beta$ SNAP deletion did not result in any detectable alterations of basic synaptic transmission and short-term plasticity (Figures S6C–S6G). Consistently, the number of synapses was not altered in  $\beta$ SNAP-KO neurons (Figures S6H and S6I).

Unlike single mutants, all DMut mice died at birth. Hippocampal neurons cultured from DMut E16–19 brains had normal morphology and synapse numbers (Figure S7). Further analyses revealed a 70% reduction in combined  $\alpha$ / $\beta$ SNAP levels in DMut

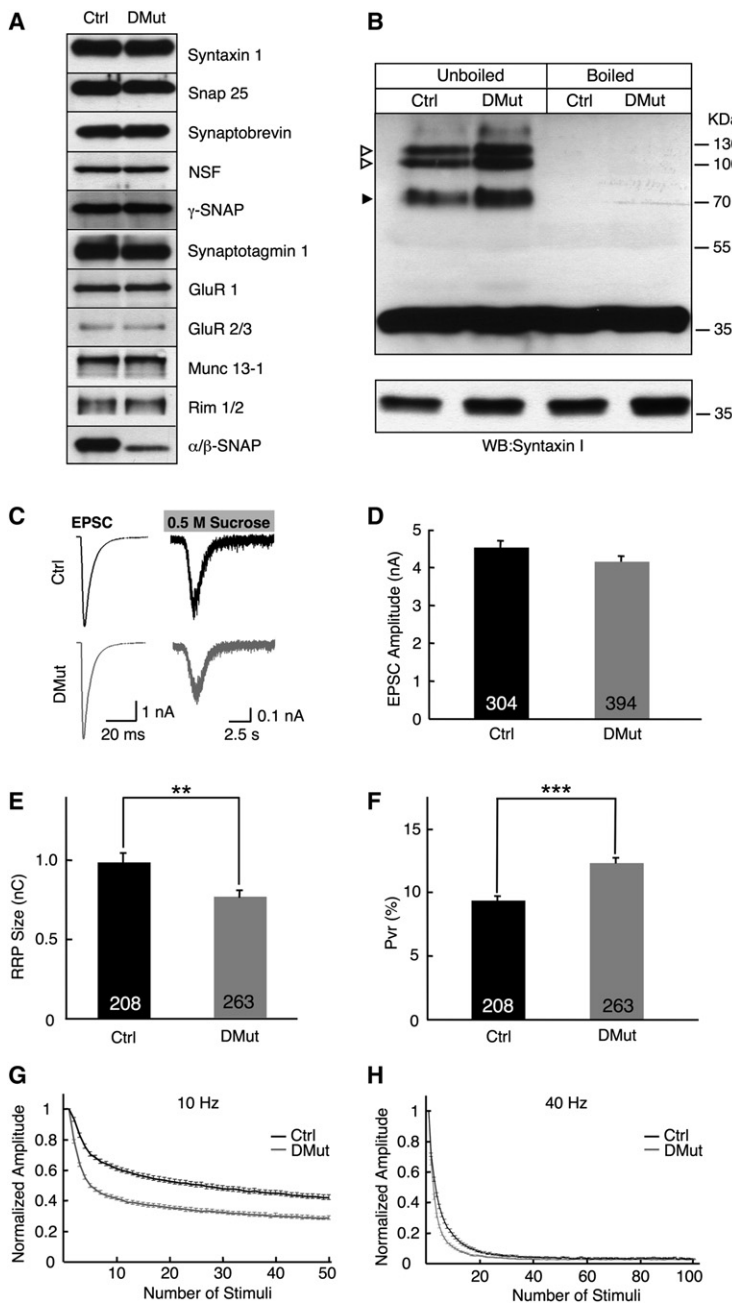


**Figure 4. Protein Expression and Synaptic Characteristics of  $\alpha/\beta$ SNAP DMut Neurons**

(A) Western blots of synaptic proteins in cultured hippocampal neurons (DIV 18-21) of Ctrl and DMut mice.

(B) Western blots for the t-SNARE Syntaxin-1 using unboiled and boiled whole-brain homogenates from Ctrl and DMut mice (E16-E19). Bands for Syntaxin-1 (37 kDa) and bands at the expected molecular weight for monomeric (filled arrowhead) and oligomeric SNARE complexes (open arrowheads) were detected.

(C) Representative EPSC traces and responses induced by HSS in Ctrl (black) and DMut (gray) neurons.

(D-F) Mean EPSC amplitude (D), RRP sizes estimated by HSS (E), and  $P_{vr}$  (F) in Ctrl and DMut neurons. Numbers in bars indicate the number of cells.

(G and H) Normalized EPSCs during 10 Hz (Ctrl, n = 234; DMut, n = 281) and 40 Hz AP trains (Ctrl, n = 151; DMut, n = 167).

Error bars indicate standard error of the mean. See also Figures S2-S8.

by an AP by the total synaptic charge triggered by HSS, was slightly increased in DMut neurons, without a change in the apparent  $Ca^{2+}$  sensitivity of evoked release (Figure 4F and Figure S8G). This increase in  $P_{vr}$  was reflected by a faster and stronger EPSC depression during AP trains that was already evident with the second stimulus of the train (Figures 4G and 4H). Thus, the 70% decrease in  $\alpha/\beta$ SNAP levels and the concomitant impairment of SNARE complex disassembly caused only a 25% reduction in the RRP at resting state with no change in synaptic release probability  $P_r$  (Figure S8D), indicating that SV fusion occurred normally. Surprisingly, however, the difference between DMut and Ctrl neurons regarding total release induced by AP trains increased with increasing stimulation strength (Figures 5A-5D). Upon 40 Hz stimulation for 2.5 s, the total release and the extrapolated RRP was some 20%-30% smaller in DMut cells as compared to Ctrl neurons (Figures 5A and 5C), much like the RRP sizes measured by HSS under resting conditions (Figures 4C and 4E). In contrast, the total release induced by a 100 Hz AP train for 9 s, the extrapolated RRP released under these conditions (Figure 5D), and the total release induced by calcimycin (Figures 5E and 5F) were reduced by ~60% in DMut cells (Ctrl,  $5.12 \pm 0.84$ , n = 21; DMut,  $1.81 \pm 0.35$ , n = 24), i.e., three times as strongly as RRP sizes estimated by HSS under resting conditions (Figures 4C and 4E).

This discrepancy, which was not due to an altered overall  $P_r$  in DMut neurons at high  $[Ca^{2+}]_i$  (Figure S8G), prompted us to monitor SV priming rates and the number of primed SVs in DMut cells by  $Ca^{2+}$  uncaging.

Fast flash-induced release was similar in Ctrl and DMut neurons (Ctrl,  $0.15 \pm 0.01$  nC; DMut,  $0.11 \pm 0.01$  nC), but the slow release phase was reduced by ~60% in DMut cells (Ctrl,  $0.88 \pm 0.14$  nC; DMut,  $0.40 \pm 0.05$  nC; Figures 6A-6D). This reduction of the slow flash-induced release phase is similar in extent to the DMut effects seen upon 100 Hz stimulation and calcimycin treatment (Figures 5D and 5F), and indicates that

brain (not shown) and cultured neurons (DMut/Ctrl ratio,  $0.30 \pm 0.09$ , n = 3; Figure 4A), no change in the expression levels of a number of candidate proteins involved in synaptic transmission (Figure 4A), and an accumulation of assembled SNARE complexes in DMut brain homogenates, indicative of a defect in SNARE complex disassembly (Figure 4B).

The RRP size in DMut neurons as determined by HSS stimulation was decreased by 25%, without changes in evoked EPSC amplitudes or mEPSC amplitudes and frequencies (Figures 4C-4E and Figures S8A-S8C). Consequently, the calculated  $P_{vr}$ , estimated by dividing the total synaptic charge triggered

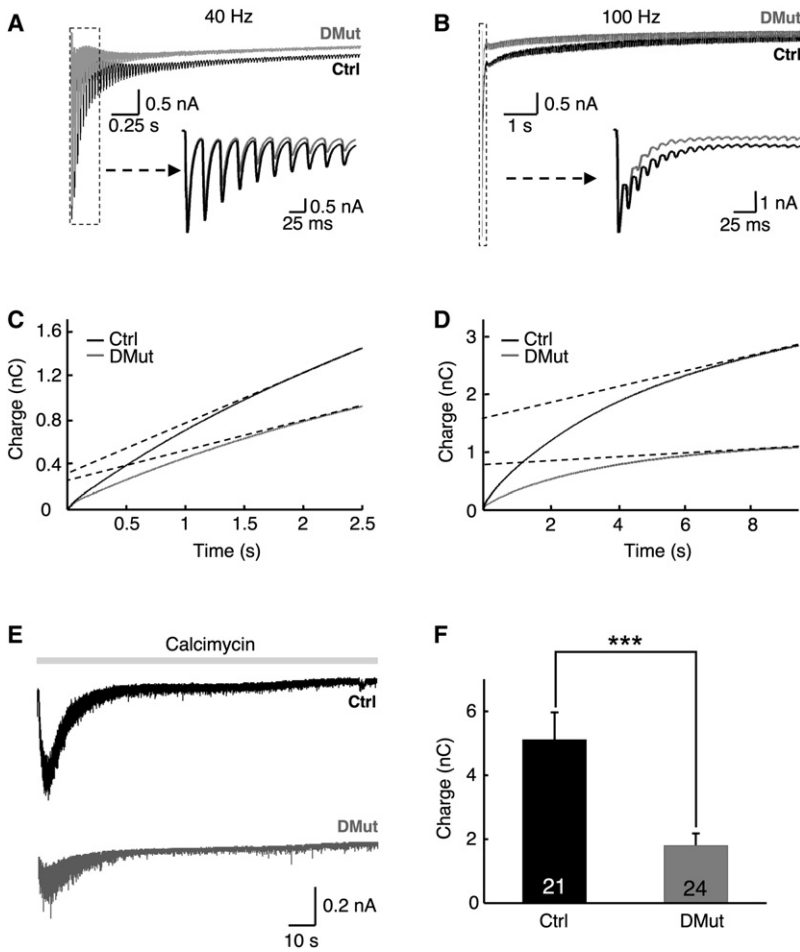


**Figure 5. Synaptic Characteristics of  $\alpha/\beta$ SNAP DMut Neurons at High  $[Ca^{2+}]_i$**

(A and B) Average EPSC traces obtained during 40 Hz (2.5 s; Ctrl, n = 151; DMut, n = 167) and 100 Hz (9 s; Ctrl, n = 20; DMut, n = 27) stimulation of Ctrl (black) and DMut (gray) neurons. The insets show magnifications of the marked sections.

(C and D) Total synaptic charge transfer calculated using the data shown in (A) and (B).

(E) Representative traces or responses to calcimycin application (10  $\mu$ M) in Ctrl (black) and DMut (gray) neurons. EPSCs that were recorded at 0.3 Hz to monitor effects of calcimycin application were removed.

(F) Total charge transfer induced by calcimycin application.

Error bars indicate standard error of the mean. See also Figures S2–S8.

the 70% reduction of  $\alpha/\beta$ SNAP levels leads to reduced levels of free SNAREs, which become rate limiting only during strong synaptic activity or when new SVs have to be primed rapidly after RRP depletion.

To discern whether the impairment of the slow flash-induced release phase in DMut neurons is due to a defect in basal RRP refilling rates or to a deficiency in the activity-dependent augmentation of SV priming (Neher and Sakaba, 2008), we measured priming rates at basal and high  $[Ca^{2+}]_i$ . We first tested  $Ca^{2+}$ -independent RRP refilling rates by applying double HSS pulses at different time intervals. RRP recovery was very similar between DMut and Ctrl neurons under these conditions (Figure 6E), indicating normal basal SV priming in DMut synapses. In addition, we found no change in Munc13-dependent priming function in DMut neurons, as assessed by the Munc13-dependent increase in transmitter release after phorbol ester stimulation (Figure S8E), or in RRP refilling as determined by seven HSS pulses given at 1 min intervals to assess SV recycling and RRP refilling over longer time scales (Figure S8F).

As basal priming rates were normal in DMut neurons, we next analyzed priming rates in the presence of elevated  $[Ca^{2+}]_i$ . Typically, SV priming into the RRP increases with increasing  $[Ca^{2+}]_i$  (Neher and Sakaba, 2008). To test if RRP refilling rates are accel-

erated similarly in DMut and Ctrl neurons by progressively increasing  $[Ca^{2+}]_i$ , we used three stimulation frequencies (10, 40, and 100 Hz) to increase  $[Ca^{2+}]_i$  and monitored EPSC recovery after RRP depletion (Figures 6F–6H). Increased stimulation frequencies cause parallel increases in  $[Ca^{2+}]_i$  in the presynaptic terminal, as temporal summation of single AP-induced  $Ca^{2+}$  transients increases due to shorter inter-stimulus intervals (Neher and Sakaba, 2008). Because a 10 Hz AP train is not sufficient to deplete the RRP, HSS was applied additionally to release all primed SVs during a continuous 10 Hz AP train. Under these conditions, DMut cells, which have the same  $P_r$  as Ctrl neurons (Figure S8D), showed an RRP recovery time course that was similar to that of Ctrl cells

(Figure 6F), indicating that the balance between exocytosis and  $Ca^{2+}$ -dependent refilling of the RRP is similar in the two genotypes. However, EPSC recovery after electrical discharge of the RRP by long 40 Hz and 100 Hz AP trains was slower in DMut neurons as compared to Ctrl cells (Figures 6G and 6H). Although the recovery time course of EPSC amplitudes from depletion is faster than that of the entire RRP (Pyott and Rosemund, 2002), it is still dependent on the restoration of the RRP in neurons with similar  $P_r$ . Thus, the slower recovery of EPSC amplitudes in DMut cells after 40 Hz or 100 Hz AP trains indicates that the activity-dependent reformation of the RRP after depletion is impaired.

We next tested if overexpression of  $\alpha$ - or  $\beta$ SNAP in DMut neurons can rescue the DMut phenotype. Both isoforms were equally efficient in restoring short-term synaptic plasticity (Figures 7A and 7B) and total release induced by 100 Hz stimuli (Figures 7C and 7D) in DMut neurons to control levels. These results indicate that the functional defects in DMut neurons are a direct consequence of the reduction in  $\alpha$ - and  $\beta$ SNAP levels, and provide additional evidence for the functional equivalence of  $\alpha$ - and  $\beta$ SNAP (see also Figures S2D and S2E).

$\alpha$ - and  $\beta$ SNAP were proposed to regulate AMPA receptor trafficking and internalization (Hanley et al., 2002). To test whether

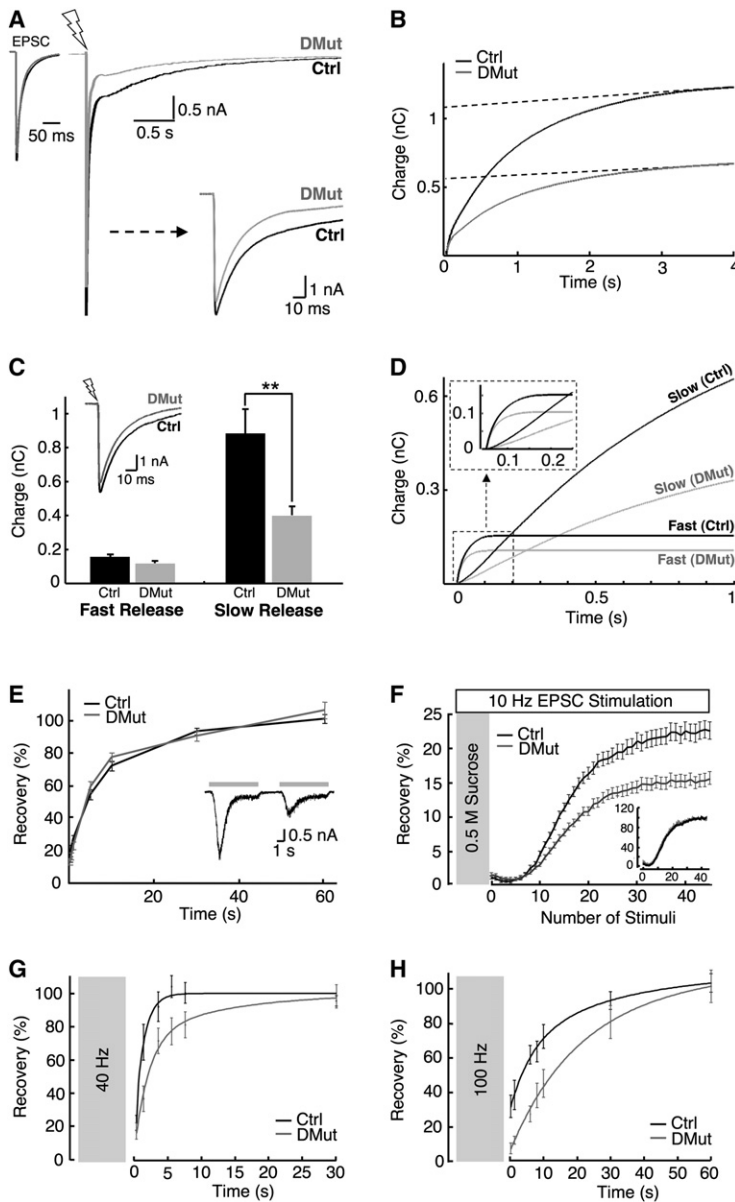


**Figure 6. SV Priming in  $\alpha/\beta$ SNAP DMut Neurons at Elevated  $[Ca^{2+}]_i$**

(A) Superimposed average flash response traces from Ctrl ( $n = 12$ ) and DMut ( $n = 15$ ) neurons. AP artifacts 200 ms after the flash were removed. The inset shows a magnification of the early phase of the flash response.

(B) Total synaptic charge transfer for data shown in (A).

(C) Total charge transfer during the fast and slow phases of the flash response in Ctrl and DMut neurons (A). The inset shows superimposed average traces for the fast release phase, obtained by subtracting slow release from total flash-induced release (as in Figure 1G).

(D) Total charge transfer for fast and slow release in Ctrl and DMut neurons (A). The inset shows a magnification of the initial 200 ms after the flash.

(E)  $Ca^{2+}$ -independent RRP refilling as measured by applying two HSS pulses at different time intervals and plotting the charge integral of the second response as percentage of the first (Ctrl,  $n = 19$ ; DMut,  $n = 14$ ). A representative trace is shown in the inset. The recovery was fitted for both Ctrl and DMut neurons with a double exponential function ( $\tau_f = 2.4$  s;  $\tau_s = 10.1$  s).

(F) The  $Ca^{2+}$ -dependent SV priming rate was measured in the presence of high  $[Ca^{2+}]_i$ . During a 10 Hz AP train, primed SVs were depleted by HSS application for 6 s, and the EPSC recovery was monitored during ongoing 10 Hz stimulation. EPSCs are normalized to the initial EPSC response (Ctrl,  $n = 127$ ; DMut,  $n = 153$ ). The inset shows EPSC responses normalized to the last response of the 10 Hz train to allow direct comparison of recovery kinetics between DMut and Ctrl neurons. The EPSC recovery was fitted with a double exponential function for both Ctrl and DMut neurons ( $\tau_f = 0.23$  s;  $\tau_s = 0.90$  s).

(G and H) Recovery of EPSC amplitudes after depletion of the RRP by 40 Hz (G) and 100 Hz (H) AP trains. After RRP discharge, SV priming into the RRP was monitored by measuring the relative recovery of EPSCs induced by single APs at different time intervals (0.25, 1.3, 6, 8, 10, 30, and 60 s). The recovery time constants after 40 Hz were 0.51 s (fast) and 1.29 s (slow) in Ctrl neurons ( $n = 17$ ) and 1.78 s and 12.19 s in DMut cells ( $n = 18$ ). The recovery time constants after 100 Hz were 6.51 s (fast) and 30.43 s (slow) in Ctrl neurons ( $n = 17$ ), and 16.89 s and 40.22 s in DMut cells ( $n = 18$ ). Error bars indicate standard error of the mean. The flash-icon indicates the flash. See also Figures S2–S8.

changes in AMPA receptor internalization contribute to the synaptic phenotypic changes we observed in DMut neurons, we probed the entire surface-expressed AMPA receptor pool of DMut and control cells by exogenous application of glutamate (10  $\mu$ M) before and 1 s after a 100 Hz AP train. Although total synaptic currents elicited by 100 Hz AP trains were drastically reduced in DMut neurons (Figure 8A), we did not observe any difference in the current responses to exogenous glutamate application between Ctrl and DMut neurons (Figures 8A and 8B) before or after the AP train. In addition, surface biotinylation experiments on  $\alpha$ - and  $\beta$ SNAP overexpressing WT neurons did not reveal any changes in the total cell surface population or in the fraction of cell surface exposed AMPA receptors containing GluR2 (data not shown). Based on these results and the fact that

mEPSC amplitudes are not altered in DMut neurons (Figure S8B), we can exclude a major contribution of postsynaptic mechanisms to the dramatic reduction in synaptic transmission in DMut neurons upon high-frequency stimulation.

In view of the above findings, and given that RRP refilling rates in DMut neurons are normal under resting conditions (Figure 6E and Figure S8F) and even during 10 Hz AP trains (Figure 6F), it is very unlikely that the apparent perturbation of RRP refilling in DMut neurons after 40 and 100 Hz stimuli is due to a defect in the priming machinery itself. Rather, our data indicate that high SV release rates require higher SV priming rates and impose a higher demand for free SNAREs in the presynaptic terminal, which become rate limiting under conditions of reduced  $\alpha/\beta$ SNAP levels and deficient SNARE complex disassembly in

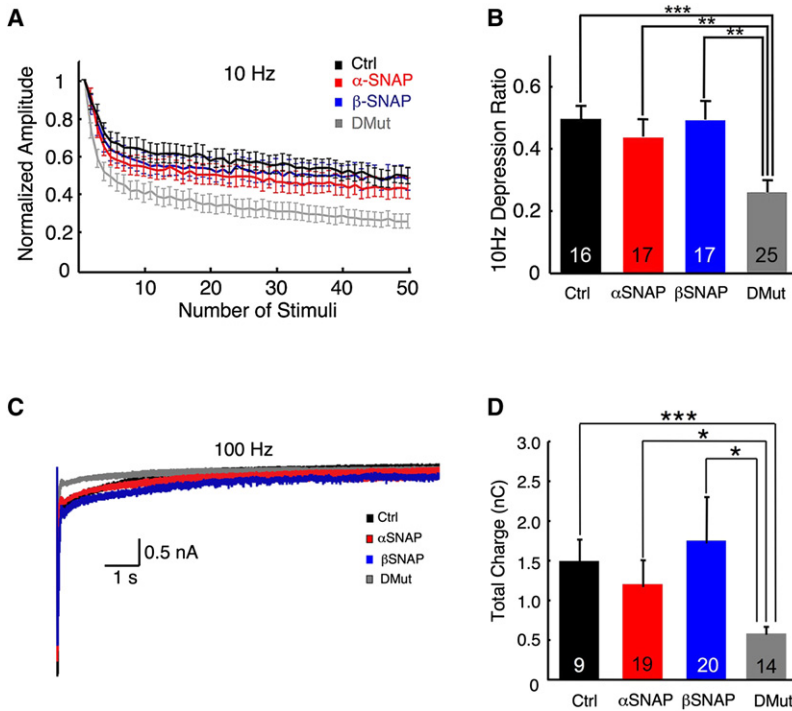


**Figure 7. Rescue of Phenotypic Changes in DMut Neurons by Overexpression of  $\alpha$ - or  $\beta$ SNAP**

(A)  $\alpha$ - (n = 17) and  $\beta$ SNAP (n = 17) were overexpressed in DMut neurons using the Semliki Forest Virus system, and short-term synaptic depression during 10 Hz stimulation was monitored. EGFP-overexpressing Ctrl (n = 16) and DMut neurons (n = 25) were used as controls. Both SNAP isoforms were able to restore 10 Hz depression to control levels.

(B) Neurons were stimulated with 50 stimuli at 10 Hz and the 10 Hz depression ratio was calculated as the ratio of the average of the last five responses during the 10 Hz train to the first response of the 10 Hz train. Numbers in the histograms indicate the numbers of cells tested.

(C) Overlaid averaged cumulative EPSC responses to 100 Hz stimulation (9 s).

(D) Total synaptic charge transfer during 100 Hz stimulation shown in (AC). Numbers in the histograms indicate the numbers of cells tested.

Error bars indicate standard error of the mean. See also Figures S2–S8.

DMut neurons, causing a retardation of RRP recovery during phases of high synaptic release activity.

## DISCUSSION

### Ca<sup>2+</sup> Uncaging in Autaptic Neurons

By Ca<sup>2+</sup> uncaging, phenomena such as SV priming, RRP heterogeneity, and SV fusion can be studied in detail and independently of Ca<sup>2+</sup> channel function, physical Ca<sup>2+</sup> channel coupling to the priming and release machineries, or Ca<sup>2+</sup> buffering. Before this study, Ca<sup>2+</sup> uncaging had not been applied to study transmitter release from small glutamatergic synapses, which are the most abundant and most frequently studied synapses in the mammalian brain. By applying the Ca<sup>2+</sup> uncaging protocol to WT, Syt-1-KO, Munc13-1/2-DKO, and CAPS1/2-DKO neurons, we made three key observations. First, asynchronous release triggered by single APs is most likely due to a change in Ca<sup>2+</sup> sensing by a sensor other than Syt-1 rather than to the presence of a unique pool of primed SVs. Second, tonic transmitter release in hippocampal glutamatergic synapses is due to ongoing priming and fusion of SVs during phases of high synaptic activity, and does not originate from a functionally distinct SV pool. Third, Syt-1 acts as a Ca<sup>2+</sup> sensor of SV fusion.

Transmitter release can be synchronous, asynchronous, or tonic, depending on the AP pattern and the spatial and temporal profile of the presynaptic [Ca<sup>2+</sup>]<sub>i</sub> elevation. Even release triggered by a single AP is often characterized by an initial synchronous phase followed by a slow asynchronous phase (Goda and Stevens, 1994), while tonic release is typically observed during high frequency AP trains as a baseline shift of synaptic release that underlies phasic release (Zucker and Lara-Estrella, 1983).

functionally distinct RRP that support the two release processes, by differences in the Ca<sup>2+</sup> sensors involved, or by a heterogeneity of SVs in the RRP due to their different coupling to Ca<sup>2+</sup> channels (Goda and Stevens, 1994; Sakaba and Neher, 2001a, 2001b; Neher and Sakaba, 2008). Tonic release, on the other hand, has been suggested to result from a build-up of asynchronous release from a distinct releasable SV pool during AP trains (Maximov and Sudhof, 2005; Sakaba, 2006). Our data show that asynchronous release, as it is for the example seen in Syt-1-KO neurons, originates from primed SVs in the RRP, whose slower release is due to the involvement of a Ca<sup>2+</sup> sensor other than Syt-1 rather than to the presence of an intrinsically distinct RRP (Figure 3; see below). In addition, our study shows that tonic release can be elicited in the complete absence of primed SVs, albeit with some delay, as is seen in the silent CAPS-DKO neurons (Figure 2). This indicates that tonic release originates from the fusion of newly primed SVs during high synaptic activity and not from an asynchronously or reluctantly releasing primed SV pool, since the latter would have been detected as a fast response by Ca<sup>2+</sup> uncaging (Wadel et al., 2007), which was not the case (Figure 2).

The notion that Syt-1 is the Ca<sup>2+</sup> sensor of SV fusion in glutamatergic forebrain synapses has been put forward in many publications. However, due to the fact that the Ca<sup>2+</sup> sensing step in these synapses has never been studied independently of Ca<sup>2+</sup> channel activation/function, the corresponding evidence has remained partially indirect, which led to alternative interpretations and criticism of the Ca<sup>2+</sup> sensor model of Syt-1 function. The present study provides direct evidence for a role of Syt-1 as the key SV Ca<sup>2+</sup> sensor in mammalian glutamatergic forebrain synapses by showing that the fast response of Syt-1-KO

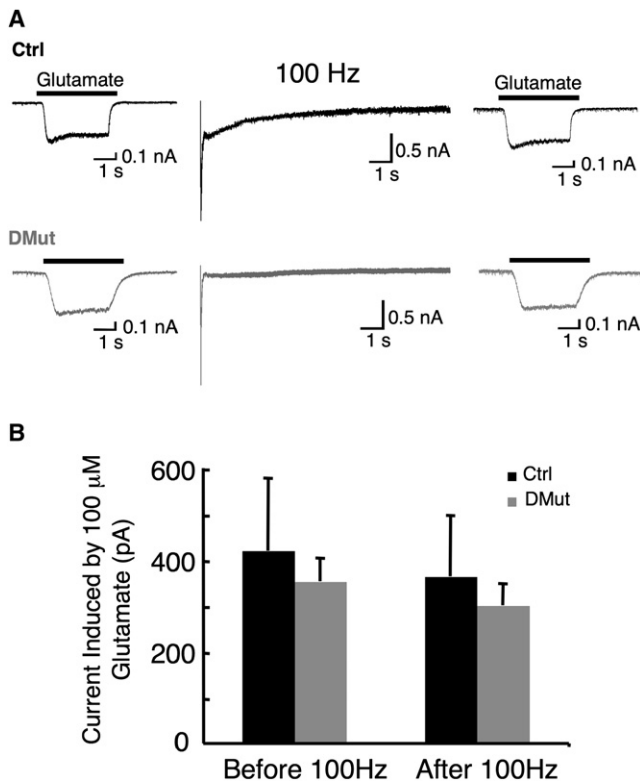


**Figure 8. Response of DMut Neurons to Exogenous Glutamate Application**

(A) Representative current responses to exogenous glutamate application (10  $\mu$ M) before and 1 s after 100 Hz stimulation in Ctrl (top) and DMut neurons (bottom). Averaged 100 Hz traces are also shown (Ctrl, n = 6; DMut, n = 7).

(B) Averaged responses to exogenous glutamate application before and after 100 Hz stimulation in Ctrl (n = 6) and DMut neurons (n = 7).

Error bars indicate standard error of the mean. See also Figures S2–S8.

neurons after flash-induced  $\text{Ca}^{2+}$  uncaging has an increased delay, a slower rise time, and a slower peak release rate (Figures 3E–3I). Further direct support for the  $\text{Ca}^{2+}$  sensor model of Syt-1 function is provided by the facts that the overall  $[\text{Ca}^{2+}]_i$  dependence of peak release rates is altered in Syt-1-KO cells, with higher release rates at low  $[\text{Ca}^{2+}]_i$  levels and lower release rates at higher  $[\text{Ca}^{2+}]_i$  levels (Figures 3H and 3I), and that even the slow phase of release triggered upon  $\text{Ca}^{2+}$  uncaging in the presence of HSS, which we interpret to be due to ongoing priming and fusion of SVs, is sensitive to Syt-1-loss (Figure S1H). In addition, we found that Syt-1 deletion mainly causes an overall kinetic slow down of release triggered by  $\text{Ca}^{2+}$  uncaging without strongly affecting the overall amount of release (Figures 3C and 3D). These findings are in accord with data on the role of Syt-2 in the calyx of Held (Sun et al., 2007) and on Syt-1 deficient autaptic cells (Liu et al., 2009). Taken together, they indicate that in the absence of Syt-1 an as yet unidentified  $\text{Ca}^{2+}$  sensor with higher  $[\text{Ca}^{2+}]_i$  sensitivity but lower efficiency is operational. The possibility that Syt-1 has an additional role in the coupling of SVs to  $\text{Ca}^{2+}$  channels and/or in SV docking (Young and Neher, 2009; de Wit et al., 2009) cannot be formally excluded on the basis of our data. However, we found that RRP sizes as

determined by HSS stimulation were similar in Syt-1-KO and control cells (Ctrl,  $0.68 \pm 0.08$  nC, n = 69; Syt-1-KO,  $0.60 \pm 0.08$  nC, n = 60), which indirectly supports the notion that SV docking and priming in hippocampal Syt-1-KO neurons are not severely altered.

### The Role of $\alpha$ - and $\beta$ SNAP in Synaptic Transmission

Our binding assays (Figures S2D and S2E) allowed us to describe four novel aspects of SNAP biochemistry. First,  $\beta$ SNAP can be incorporated into the 20S complex and can participate in its NSF-dependent disassembly via ATP hydrolysis. Second, mixed 20S complexes containing both SNAPs as well as complexes containing either  $\alpha$ - or  $\beta$ SNAP are formed with similar efficiency. Third,  $\alpha$ - and  $\beta$ SNAP do not have different synaptic interaction partners. These findings indicate that  $\alpha$ - and  $\beta$ SNAP have similar and largely redundant functions in synapses, which is further supported by the fact that neither the deletion of  $\beta$ SNAP in KO neurons (Figure S6) nor the reduction of  $\alpha$ SNAP levels in HYH neurons (Figure S5) affect nerve cell viability, differentiation, or function.

The reduction of the combined  $\alpha/\beta$ SNAP levels by 70%, as observed in the DMut neurons, has no detectable effect on cell morphogenesis and differentiation (Figure S7). This finding is surprising in view of the essential role of SNAPs in multiple cellular vesicle trafficking pathways, and indicates that  $\alpha/\beta$ SNAP levels in hippocampal neurons are far supersaturating. This is supported by the observations that overexpression of  $\alpha$ - or  $\beta$ SNAP in WT neurons (Figure S3), deletion of  $\beta$ SNAP in KO neurons (Figure S6), or reduction of  $\alpha$ SNAP levels in HYH neurons (Figure S5) do not affect nerve cell development or synaptic transmission either. In this regard, it is important to note that our overexpression data (Figure S3) contradict earlier studies, which indicated that increases of SNAP levels above WT levels promote transmitter release (He et al., 1999) and alter AMPA receptor trafficking (Hanley et al., 2002). In principle, these discrepancies could be due to different absolute and relative expression levels of  $\alpha/\beta$ SNAP, NSF, and SNAREs and/or their differential subcellular distribution in different cell types and tissue preparations.

Even if the combined  $\alpha/\beta$ SNAP levels are reduced by 70%, as is the case in DMut neurons, basic synaptic transmission is hardly affected (Figures 4C–4F). Only if synapses are stimulated at high frequency (Figures 4G, 4H, and 5B) or by strong and persistent increases in  $[\text{Ca}^{2+}]_i$  after calcimycin treatment (Figures 5E and 5F) or  $\text{Ca}^{2+}$  uncaging (Figures 6A–6D), a defect in synaptic transmission becomes manifest in DMut neurons. At the same time, the basal function of key priming proteins of the Munc13 family is unperturbed in these neurons, and the apparent SV priming rate is only reduced upon very strong stimulation, when priming rates are upregulated due to the increased  $[\text{Ca}^{2+}]_i$  (Figures 6G and 6H). A defect in  $\text{Ca}^{2+}$  sensitivity at DMut synapses cannot account for the DMut phenotype as the apparent  $\text{Ca}^{2+}$  sensitivity of release at DMut synapses is unaltered (Figure S8G).

The synaptic phenotype of the DMut neurons described here is different from that seen at neuromuscular junctions of hemizygous/hypomorphic *Drosophila* SNAP mutants (Babcock et al., 2004), where the amplitude of miniature excitatory junctional

potentials (EJPs) is increased (compare to Figure S8B), the quantal content of evoked EJPs is reduced (compare to Figure 4D and Figure S8B), and evoked EJPs during 10 Hz stimulation trains are not altered (compare to Figure 4G). Based on our data, we conclude that  $\alpha$ - and  $\beta$ SNAP do not affect SV priming as such but rather determine the availability of free SNARE proteins as priming substrates. This substrate limitation, in turn, affects SV priming rates. Such a role of  $\alpha$ - and  $\beta$ SNAP would also explain the strongly reduced tonic release rate in  $\alpha/\beta$ SNAP DMut cells (Figures 5A and 5B) because tonic release represents ongoing priming and fusion of SVs and hence the availability of free SNAREs is predicted to be one of its key determinants.

Essentially, almost all phenotypic changes that we observed in  $\alpha/\beta$ SNAP DMut synapses can be explained by a postfusion function of  $\alpha$ - and  $\beta$ SNAP in SNARE complex disassembly. Based on our data, we can exclude that  $\beta$ SNAP has a specific role in the regulation of Syt-1 function that is not shared by  $\alpha$ SNAP. Such a role for  $\beta$ SNAP was suggested earlier (Schiavo et al., 1995) but is not compatible with our finding that  $\beta$ SNAP-KO neurons do not show any detectable phenotypic alterations in synaptic transmission (Figure S6). Likewise, the lack of phenotypic synaptic changes after  $\beta$ SNAP-KO (Figure S6) or  $\beta$ SNAP overexpression (Figure S3), and the unaltered surface-expressed AMPA receptor pool in DMut neurons (Figure 8) is incompatible with a distinct role of only  $\beta$ SNAP, but not  $\alpha$ SNAP, in AMPA receptor internalization (Hanley et al., 2002). In fact, our analysis of hippocampal  $\beta$ SNAP-KO neurons indicates that  $\beta$ SNAP does not have any specific synaptic function in these neurons that cannot be compensated for by  $\alpha$ SNAP. The only finding that might require an extension of the interpretation of a pure postfusion function of  $\alpha$ - and  $\beta$ SNAP in SNARE complex disassembly is that  $P_{vr}$  is slightly increased in DMut neurons, without changes in the apparent  $Ca^{2+}$  sensitivity of evoked release (Figure 4F and Figure S8G). This increase in  $P_{vr}$  was also reflected by a faster and stronger EPSC depression during AP trains, which was already evident with the second stimulus of the train (Figures 4G and 4H), and might indicate an additional rapid action of the  $\alpha/\beta$ SNAP-NSF system before SV fusion (Kuner et al., 2008).

Given that DMut neurons still express  $\alpha$ SNAP at 50% of the WT levels, we cannot formally exclude, based on the selective defect in SV priming in DMut neurons, that  $\alpha$ - and  $\beta$ SNAP play additional and redundant roles in synaptic function that went undetected in our study. A more stringent genetic analysis of such additional  $\alpha/\beta$ SNAP functions is impossible because the complete genetic elimination of  $\alpha$ SNAP is embryonically lethal (Chae et al., 2004), and a complete genetic or RNAi-induced elimination of  $\alpha$ - and  $\beta$ SNAP is likely to be incompatible with early embryonic and nerve cell survival because the  $\alpha/\beta$ SNAP-NSF complex has essential roles in multiple intracellular trafficking pathways (e.g., in Golgi trafficking) whose arrest would confound an analysis of synaptic function in neurons (Babcock et al., 2004).

## EXPERIMENTAL PROCEDURES

Further details on the experimental procedures described below are given in the Supplemental Experimental Procedures.

### Cell Culture and Electrophysiology

Autaptic cultures of hippocampal neurons were prepared on 200  $\mu$ m  $\times$  200  $\mu$ m substrate islands. Cells were whole-cell patch clamped at  $-70$  mV. EPSCs were evoked by depolarization of the cell membrane potential from  $-70$  to 0 mV for 2 ms. RRP sizes were determined by application of 0.5 M sucrose solution. High voltage activated  $Ca^{2+}$  currents were recorded in the presence of nimodipine (Sigma). The  $n$  values for electrophysiological recordings indicate the number of cells tested. Error bars indicate standard errors of the mean. Statistical significance was tested using Student's  $t$  test.

### $Ca^{2+}$ Uncaging and Measurements of $[Ca^{2+}]_i$

For  $Ca^{2+}$  uncaging experiments, single light pulses were generated by a UV flash lamp (Rapp OptoElectronics) and coupled into the epifluorescence port of an inverted microscope.  $[Ca^{2+}]_i$  was monitored in distal dendrites (third order branches) by Mag-Fura-2 and Fura-4F (Invitrogen), which were excited at 360/380 nm by a monochromator (TILL Photonics). The emitted fluorescence was collected with a photodiode (TILL Photonics).  $Ca^{2+}$  imaging was performed by collecting fluorescence with a CCD camera (VGA; PCO). The recording extracellular solution contained CTZ to prevent AMPA receptor desensitization and  $\gamma$ DGG to block AMPA receptor saturation. For measurements of  $[Ca^{2+}]_i$ , Mag-Fura-2 and Fura-4F were added to the patch pipette. Deconvolution of EPSCs triggered by  $Ca^{2+}$  uncaging were carried out using a measured mEPSC waveform as described previously (van der Kloot, 1988). The  $n$ -values for all recordings indicate the number of cells tested. Error bars indicate standard errors of the mean. Statistical significance was tested using Student's  $t$  test. The relationship between local  $[Ca^{2+}]_i$  and release was modeled using a five-site kinetic model (Schneppenburger and Neher, 2000).  $Ca^{2+}$  binding and unbinding rates were estimated using a Runge-Kutta algorithm to numerically solve the system of coupled differential equations (Schneppenburger and Neher, 2000; Wadel et al., 2007). Nonlinear least-square fitting of release rate versus  $[Ca^{2+}]_i$  scatter plots was performed using the Levenberg-Marquardt minimization algorithm (Schneppenburger and Neher, 2000).

### Western Blotting and SNARE Complex Analysis

Protein levels in brain homogenates and lysates of cultured hippocampal neurons were analyzed by immunoblotting. Quantification was performed densitometrically or by detection of fluorescently labeled secondary antibodies using an Odyssey infrared scanner (LI-COR Biotechnology). SNARE complex analysis was performed as described previously (Otto et al., 1997; Tolar and Pallanck, 1998; Xu and Bajjalieh, 2001).

### Mutant Mouse Lines

$\beta$ SNAP-KO mice were generated by homologous recombination in embryonic stem cells. In the  $\beta$ SNAP targeting vector, the first coding exon was replaced by a neomycin resistance cassette (Figure S4A).  $HYH$  mice were provided by Dr. C.A. Walsh (Boston, MA) (Chae et al., 2004).

### Morphological Analyses

Autaptic neuronal cultures were fixed (4% PFA) at 9–15 DIV. For the morphological analysis of dendrites, neurons were stained with a mouse-anti-MAP2 (Chemicon) antibody. To identify excitatory synapses, guinea-pig-anti-vGluT1 (Chemicon) in combination with mouse-anti-PSD95 (Transduction Laboratories) or mouse-anti-Synapsin (Synaptic Systems) antibodies were used.

### Recombinant Protein Expression and Purification and Pull-Down Assays

Expression, purification, and storage of recombinant Myc-tagged NSF, His<sub>6</sub>-tagged  $\alpha$ - and  $\beta$ SNAP were performed according to published procedures (Barszczewski et al., 2008). For pull-down experiments, Triton X-100 solubilized brain membranes were prepared from WT mice. Triton X-100 extracts and purified recombinant NSF were incubated in the presence of recombinant  $\alpha$ - or  $\beta$ SNAP. The binding reaction was allowed to proceed for 1–2 hr at 4°C. Then anti-Myc antibody 9E10 (Sigma-Aldrich) was added, and the reaction was allowed to proceed for an additional 2 hr at 4°C. Protein-G coupled beads (Pharmacia Biotech) were added to each tube, and incubated for 2 hr. Beads were collected by centrifugation, washed with solubilization

buffer, and eluted with ATP/Mg<sup>2+</sup> elution buffer. Eluted fractions were analyzed by SDS-PAGE and western blotting or by mass spectrometry.

### SUPPLEMENTAL INFORMATION

Supplemental Information includes Supplemental Experimental Procedures and eight figures and can be found with this article online at [doi:10.1016/j.neuron.2010.09.019](https://doi.org/10.1016/j.neuron.2010.09.019).

### ACKNOWLEDGMENTS

We thank F. Bensele, A. Galinski, T. Hellmann, I. Thanhäuser, D. Schwerdtfeger, and the staff of our Transgenic Animal Facility for invaluable support. We thank D. Fasshauer for SNAP and NSF expression plasmids, and E. Neher and H. Betz for advice and critical comments on the manuscript. This work was supported by the Max Planck Society and the European Community (Marie Curie NEUREST fellowship MEST-CT-2004-504193 to A.B.).

Accepted: August 26, 2010

Published: November 3, 2010

### REFERENCES

- Babcock, M., Macleod, G.T., Leither, J., and Pallanck, L. (2004). Genetic analysis of soluble N-ethylmaleimide-sensitive factor attachment protein function in *Drosophila* reveals positive and negative secretory roles. *J. Neurosci.* *24*, 3964–3973.
- Barszczewski, M., Chua, J.J., Stein, A., Winter, U., Heintzmann, R., Zilly, F.E., Fasshauer, D., Lang, T., and Jahn, R. (2008). A novel site of action for alpha-SNAP in the SNARE conformational cycle controlling membrane fusion. *Mol. Biol. Cell* *19*, 776–784.
- Chae, T.H., Kim, S., Marz, K.E., Hanson, P.I., and Walsh, C.A. (2004). The HYH mutation uncovers roles for alpha Snap in apical protein localization and control of neural cell fate. *Nat. Genet.* *36*, 264–270.
- Clary, D.O., Griff, I.C., and Rothman, J.E. (1990). SNAPs, a family of NSF attachment proteins involved in intracellular membrane fusion in animals and yeast. *Cell* *61*, 709–721.
- de Wit, H., Walter, A.M., Milosevic, I., Gulyas-Kovacs, A., Riedel, D., Sorensen, J.B., and Verhage, M. (2009). Synaptotagmin-1 docks secretory vesicles to syntaxin-1/SNAP-25 acceptor complexes. *Cell* *138*, 935–946.
- DeBello, W.M., O'Connor, V., Dresbach, T., Whiteheart, S.W., Wang, S.S., Schweizer, F.E., Betz, H., Rothman, J.E., and Augustine, G.J. (1995). SNAP-mediated protein-protein interactions essential for neurotransmitter release. *Nature* *373*, 626–630.
- Geppert, M., Goda, Y., Hammer, R.E., Li, C., Rosahl, T.W., Stevens, C.F., and Sudhof, T.C. (1994). Synaptotagmin I: A major Ca<sup>2+</sup> sensor for transmitter release at a central synapse. *Cell* *79*, 717–727.
- Goda, Y., and Stevens, C.F. (1994). Two components of transmitter release at a central synapse. *Proc. Natl. Acad. Sci. USA* *91*, 12942–12946.
- Hagler, D.J., Jr., and Goda, Y. (2001). Properties of synchronous and asynchronous release during pulse train depression in cultured hippocampal neurons. *J. Neurophysiol.* *85*, 2324–2334.
- Hanley, J.G., Khatri, L., Hanson, P.I., and Ziff, E.B. (2002). NSF ATPase and alpha-/beta-SNAPs disassemble the AMPA receptor-PICK complex. *Neuron* *34*, 53–67.
- He, P., Southard, R.C., Chen, D., Whiteheart, S.W., and Cooper, R.L. (1999). Role of alpha-SNAP in promoting efficient neurotransmission at the crayfish neuromuscular junction. *J. Neurophysiol.* *82*, 3406–3416.
- Hefft, S., and Jonas, P. (2005). Asynchronous GABA release generates long-lasting inhibition at a hippocampal interneuron-principal neuron synapse. *Nat. Neurosci.* *8*, 1319–1328.
- Hong, H.K., Chakravarti, A., and Takahashi, J.S. (2004). The gene for soluble N-ethylmaleimide sensitive factor attachment protein alpha is mutated in hydrocephaly with hop gait (HYH) mice. *Proc. Natl. Acad. Sci. USA* *101*, 1748–1753.
- Jahn, R., and Scheller, R.H. (2006). SNAREs—engines for membrane fusion. *Nat. Rev. Mol. Cell Biol.* *7*, 631–643.
- Jockusch, W.J., Speidel, D., Sigler, A., Sorensen, J.B., Varoqueaux, F., Rhee, J.S., and Brose, N. (2007). CAPS-1 and CAPS-2 are essential synaptic vesicle priming proteins. *Cell* *131*, 796–808.
- Kuner, T., Li, Y., Gee, K.R., Bonewald, L.F., and Augustine, G.J. (2008). Photolysis of a caged peptide reveals rapid action of N-ethylmaleimide sensitive factor before neurotransmitter release. *Proc. Natl. Acad. Sci. USA* *105*, 347–352.
- Littleton, J.T., Barnard, R.J., Titus, S.A., Slind, J., Chapman, E.R., and Ganetzky, B. (2001). SNARE-complex disassembly by NSF follows synaptic-vesicle fusion. *Proc. Natl. Acad. Sci. USA* *98*, 12233–12238.
- Liu, H., Dean, C., Arthur, C.P., Dong, M., and Chapman, E.R. (2009). Autapses and networks of hippocampal neurons exhibit distinct synaptic transmission phenotypes in the absence of synaptotagmin I. *J. Neurosci.* *29*, 7395–7403.
- Martin, H.G., Henley, J.M., and Meyer, G. (2006). Novel putative targets of N-ethylmaleimide sensitive fusion protein (NSF) and alpha/beta soluble NSF attachment proteins (SNAPs) include the Pak-binding nucleotide exchange factor betaPIX. *J. Cell. Biochem.* *99*, 1203–1215.
- Maximov, A., and Sudhof, T.C. (2005). Autonomous function of synaptotagmin 1 in triggering synchronous release independent of asynchronous release. *Neuron* *48*, 547–554.
- McMahon, H.T., Missler, M., Li, C., and Sudhof, T.C. (1995). Complexins: Cytosolic proteins that regulate SNAP receptor function. *Cell* *83*, 111–119.
- Morgan, A., and Burgoyne, R.D. (1995). A role for soluble NSF attachment proteins (SNAPs) in regulated exocytosis in adrenal chromaffin cells. *EMBO J.* *14*, 232–239.
- Neher, E., and Sakaba, T. (2008). Multiple roles of calcium ions in the regulation of neurotransmitter release. *Neuron* *59*, 861–872.
- Nishiki, T., Nihonmatsu, I., Tsuhara, Y., Kawasaki, M., Sekiguchi, M., Sato, K., Mizoguchi, A., and Takahashi, M. (2001). Distribution of soluble N-ethylmaleimide fusion protein attachment proteins (SNAPs) in the rat nervous system. *Neuroscience* *107*, 363–371.
- Otsu, Y., Shahrezaei, V., Li, B., Raymond, L.A., Delaney, K.R., and Murphy, T.H. (2004). Competition between phasic and asynchronous release for recovered synaptic vesicles at developing hippocampal autaptic synapses. *J. Neurosci.* *24*, 420–433.
- Otto, H., Hanson, P.I., and Jahn, R. (1997). Assembly and disassembly of a ternary complex of synaptobrevin, syntaxin, and SNAP-25 in the membrane of synaptic vesicles. *Proc. Natl. Acad. Sci. USA* *94*, 6197–6201.
- Peter, F., Wong, S.H., Subramaniam, V.N., Tang, B.L., and Hong, W. (1998). Alpha-SNAP but not gamma-SNAP is required for ER-Golgi transport after vesicle budding and the Rab1-requiring step but before the EGTA-sensitive step. *J. Cell Sci.* *111*, 2625–2633.
- Pyott, S.J., and Rosenmund, C. (2002). The effects of temperature on vesicular supply and release in autaptic cultures of rat and mouse hippocampal neurons. *J. Physiol.* *539*, 523–535.
- Sakaba, T. (2006). Roles of the fast-releasing and the slowly releasing vesicles in synaptic transmission at the calyx of held. *J. Neurosci.* *26*, 5863–5871.
- Sakaba, T. (2008). Two Ca<sup>2+</sup>-dependent steps controlling synaptic vesicle fusion and replenishment at the cerebellar basket cell terminal. *Neuron* *57*, 406–419.
- Sakaba, T., and Neher, E. (2001a). Calmodulin mediates rapid recruitment of fast-releasing synaptic vesicles at a calyx-type synapse. *Neuron* *32*, 1119–1131.
- Sakaba, T., and Neher, E. (2001b). Quantitative relationship between transmitter release and calcium current at the calyx of held synapse. *J. Neurosci.* *21*, 462–476.

- Schiavo, G., Gmachl, M.J., Stenbeck, G., Sollner, T.H., and Rothman, J.E. (1995). A possible docking and fusion particle for synaptic transmission. *Nature* 378, 733–736.
- Schneggenburger, R., and Neher, E. (2000). Intracellular calcium dependence of transmitter release rates at a fast central synapse. *Nature* 406, 889–893.
- Sollner, T., Bennett, M.K., Whiteheart, S.W., Scheller, R.H., and Rothman, J.E. (1993). A protein assembly-disassembly pathway in vitro that may correspond to sequential steps of synaptic vesicle docking, activation, and fusion. *Cell* 75, 409–418.
- Sudhof, T.C. (2004). The synaptic vesicle cycle. *Annu. Rev. Neurosci.* 27, 509–547.
- Sun, J., Pang, Z.P., Qin, D., Fahim, A.T., Adachi, R., and Sudhof, T.C. (2007). A dual- $\text{Ca}^{2+}$ -sensor model for neurotransmitter release in a central synapse. *Nature* 450, 676–682.
- Tolar, L.A., and Pallanck, L. (1998). NSF function in neurotransmitter release involves rearrangement of the SNARE complex downstream of synaptic vesicle docking. *J. Neurosci.* 18, 10250–10256.
- van der Kloot, W. (1988). Estimating the timing of quantal releases during end-plate currents at the frog neuromuscular junction. *J. Physiol.* 402, 595–603.
- Wadel, K., Neher, E., and Sakaba, T. (2007). The coupling between synaptic vesicles and  $\text{Ca}^{2+}$  channels determines fast neurotransmitter release. *Neuron* 53, 563–575.
- Whiteheart, S.W., Griff, I.C., Brunner, M., Clary, D.O., Mayer, T., Buhrow, S.A., and Rothman, J.E. (1993). SNAP family of NSF attachment proteins includes a brain-specific isoform. *Nature* 362, 353–355.
- Wojcik, S.M., and Brose, N. (2007). Regulation of membrane fusion in synaptic excitation-secretion coupling: Speed and accuracy matter. *Neuron* 55, 11–24.
- Xu, J., Xu, Y., Ellis-Davies, G.C., Augustine, G.J., and Tse, F.W. (2002). Differential regulation of exocytosis by alpha- and beta-SNAPs. *J. Neurosci.* 22, 53–61.
- Xu, T., and Bajjalieh, S.M. (2001). SV2 modulates the size of the readily releasable pool of secretory vesicles. *Nat. Cell Biol.* 3, 691–698.
- Young, S.M., and Neher, E. (2009). Synaptotagmin has an essential function in synaptic vesicle positioning for synchronous release in addition to its role as a calcium sensor. *Neuron* 63, 482–496.
- Zucker, R.S., and Lara-Estrella, L.O. (1983). Post-tetanic decay of evoked and spontaneous transmitter release and a residual-calcium model of synaptic facilitation at crayfish neuromuscular junctions. *J. Gen. Physiol.* 81, 355–372.